Available online at www.sciencedirect.com
ScienceDirect
Journal of Photochemistry and Photobiology A: Chemistry 184 (2006) 313–321
Journal of Photochemistry and Photobiology A:Chemistry
www.elsevier.com/locate/jphotochem

Photocatalytic microbial inactivation over Pd doped SnO_2 and TiO_2 thin films

Arcan Erkan, Ufuk Bakir, Gurkan Karakas *

Middle East Technical University, Chemical Engineering Department, 06531 Ankara, Turkey

Received 29 December 2005; received in revised form 20 April 2006; accepted 2 May 2006
Available online 16 May 2006

Abstract

The photocatalytic antimicrobial activity over TiO_2, SnO_2 and their Pd doped thin film samples were determined against *Escherichia coli*, *Staphylococcus aereus*, *Saccharomyces cerevisiae* and *Aspergilus niger* spores. Higher antimicrobial activity was observed with TiO_2 than SnO_2 thin films and, Pd addition contributes to an increase in the activity of both semiconductor oxides. The highest microbial inactivation was achieved with 1% PdO/TiO_2 against *E. coli* with a 98% decrease in survival after 2 h illumination. SnO_2 was found to show lower photocatalytic efficiency against *E. coli* with a 56% decrease in survival after 2 h illumination and a 68% decrease in survival of *E. coli* after palladium addition. *E. coli* showed the least and *S. cerevisiae* showed the highest resistance against photocatalytic inactivation and, *A. niger* spores could not be inactivated up to 8 h illumination over all the surfaces. The antimicrobial efficiencies against different microorganisms and fungal spores were found to decrease in the following order: *E. coli* > *S. aereus* > *S. cerevisiae* > *A. niger* spores for which, complexity and strength of the cell walls increased in the same order.

Keywords: Photocatalytic inactivation; Antimicrobial surfaces; Palladium; TiO_2; SnO_2; Sol–gel; *E. coli*; *S. aereus*; *S. cerevisiae*; *A. niger* spores

1. Introduction

Microbial contamination and growth on the surfaces are potential risks for human health. The use of aggressive chemicals such as detergents, alcohols and chlorine components for manual disinfection is not environmentally benign and is ineffective for long-term disinfection. The UV radiation is an effective, but temporary photochemical method for disinfection, which requires special irradiation source within UV-C (185–254 nm) band. However, the hazards of intensive and direct use of UV radiation limits its application to medical and technical purposes only. Photocatalysis is an alternative to direct UV disinfection and, considerable antimicrobial efficacy is possible with higher wavelengths, which are naturally present in ambient solar and artificial light. Large band gap semiconductors, such as TiO_2, SnO_2, and ZnO, are suitable photocatalytic materials with their higher wavelength UV absorption (UV-A, 320–400 nm) and have found great interest on wide range of applications such as, direct splitting of water for hydrogen production, partial or complete photocatalytic oxidation of organic materials and disinfection of microorganisms [1–6]. Photocatalytic microbial inactivation was first reported by Matsunaga et al. more than 20 years ago [1]. In that study, *Lactobacillus acidophilus, Saccharomyces cerevisiae* and *Escherechia coli* were completely inactivated with the use of Pt-loaded TiO_2 powder and the cell inactivation mechanism was explained with the oxidation of coenzyme A and the inhibition of respiration. Since then, many photocatalytic inactivation studies have been conducted on a wide spectrum of organisms including cancer cells, phages, viruses, bacteria, fungi, algae and protozoa [6–20]. Generally TiO_2 [6–19], but in a few cases ZnO [19,20], was examined as semiconductor photocatalyst, and the effects of Cu and Al addition as dopants on photocatalytic microbial inactivation were also investigated [21,22]. Besides, the effects of semiconductor concentration, light intensity, temperature [8], particle size [23], pH [24], microorganism type [25,15] and humidity [15] were also reported.

The photocatalytic reaction mechanism is initiated by the absorption of UV light which, results in the promotion of an electron from the valence band to the conduction band. When

* Corresponding author. Tel.: +90 312 2102630; fax: +90 312 2102600.
E-mail address: gkarakas@metu.edu.tr (G. Karakas).

1010-6030/$ – see front matter © 2006 Elsevier B.V. All rights reserved.
doi:10.1016/j.jphotochem.2006.05.001

the electron is transferred to the empty conduction band, electron/hole (e^-/h^+) pairs are formed within the semiconductor materials. The electron/hole pairs move to the surface as a result of charge separation where, electrons reduce oxygen to superoxide radicals ($^\bullet O_2^-$) and further reaction with H_2O molecules yield OH^- ions. Both OH^- ions and H_2O molecules are converted to $^\bullet OH$ radicals by reacting with the holes. Both hydroxyl and oxygen radicals are capable of performing many selective/nonselective oxidation reactions [5,26–32]. The photocatalytic microbial inactivation has been reported in number of studies for different microorganisms and cell cultures and; explained by different mechanisms such as cell membrane and the wall damage [13,20,21,23,33], physicochemical alteration of the cell membrane [34], promotion of cell membrane permeability to Ca^{2+} [35], reduction of intracellular superoxide dismutase activity (a protective enzyme from oxidative stress) [36] and abnormal cell division [34]. Hydroxyl radical has been reported as the major oxidant [9,10,28] but, other reactive oxygen species, such as H_2O_2, O^{2-}, were also shown responsible of oxidation [11,24,30]. Cho et al. [7] reported the dependence of reactive oxidation radicals on the type of the cells or phage [7]. Inactivation of MS-2 phage was carried out predominantly through the action of the bulk phase free hydroxyl radical, but that *E. coli* was inactivated by both free and surface-bound hydroxyl radicals and O^{2-} and H_2O_2.

The efficiency of photocatalysts can be elucidated as the ratio of photon absorption rate to the generation rate of free radicals. However, the recombination of holes with electrons usually takes place within a solid matrix, and only a small fraction of electrons and holes can exceed the charge carrier length, and reach to the surface. Therefore, electron/hole recombination within the volume of the particles and the transport of electrons and holes through charge carrier length are the main limiting steps between the generation step of electron/hole pairs and the production rate of reactive free radicals. Synthetically produced semiconductor materials with higher surface area to volume ratio and porosity improve the photocatalytic efficiency by increasing the number of photon absorption per unit irradiated area [37,38]. Similarly, the use of smaller particle size, which is less than carrier length, improves the photocatalytic efficiency by decreasing electron/hole recombination probability. In addition, particles consisting of smaller crystallite size produce higher number of electron/hole pairs with indirect band transition mechanism. The charge carrier length for TiO_2 was reported as 100 nm hence, larger particles will yield poor photocatalytic efficiency, which is in the order of 5% for most applications utilizing pure semiconductor metal oxides [38–41]. The presence of trace metal ion impurities or addition of dopants also play an important role on optical, electronic and chemical properties of semiconductors. The finely dispersed transition metal ions such as Au^{3+}, Ag^+, Nb^{3+}, V^{2+}, Pt^{4+}, and Pd^{2+} within the semiconductor metal oxide and over the surface act as electron/hole traps, which exhibit Schottky effect and inhibit recombination probability of electron/hole pairs [1,42–47]. However, the dispersion of metal ion centers within the lattice and over the surface of semiconductors may have a negative affect because of the coarse and improperly dispersed dopant crystallites also acting as recombination centers. In addition, the transition metal oxides enhance the surface reaction rates with their unique oxidation–reduction potential at moderate temperatures. The platinum group metals, such as Pd and Pt, over semiconductor metal oxide supports promote many oxidation and reduction reactions depending on their oxidation state and the synergistic effect was elaborated with different mechanisms. Spillover of activated surface species from metal oxide to support [48–50], oxygen spillover from semiconductor metal oxide support to metal [51,52], formation of alloys between precious metal dopant and support [52–54] have been well documented to explain the metal–support interactions and the resulting synergistic effect on the catalytic activity. In addition to the synergistic effects of platinum group metals, palladium and platinum doping of TiO_2 also enhances the photocatalytic oxidation of hydrocarbons and promising results on the photocatalytic oxidation of 2-clorophenol [42], 1-propanol and 1,2-propanediol [47], formic acid [55] and organic pigments [56] were reported in literature. However, the effect of palladium as dopant over the photocatalytic inactivation of microorganisms has not been reported in literature.

In the present study, the effect of palladium promotion on the photocatalytic inactivation of *E. coli*, *S. aereus*, *S. cerevisia* and *A. niger* spores over TiO_2 and SnO_2 thin films were studied. Although the photocatalytic efficiency of TiO_2 is higher than SnO_2, the effect of palladium on the photocatalytic inactivation of microorganisms was also validated with SnO_2 thin films.

2. Materials and methods

2.1. Substrate preparation

Thin films of TiO_2, SnO_2, Pd–TiO_2 and Pd–SnO_2 were deposited over Pyrex glass plates by a dip coating technique. Prior to coating, the glass plates (25 mm × 75 mm × 1 mm) were washed with detergent solution, were rinsed with distilled water and, pretreated with saturated NaOH solution for 5 min. The pretreated glass substrates were rinsed with distilled water and finally ultrasonicated in ethanol–chloroform (1:1, v/v) solution for 10 min and were dried at 110 °C overnight. The TiO_2 sols were prepared by using titanium tetraisopropoxide (TTIP, Aldrich, extra pure grade), ethanol (C_2H_5OH, 99.5%) and 35% $HCl_{aq.}$ without further purification. TTIP (8.4 ml) was first dissolved in ethanol (20 ml) and hydrolyzed with drop wise addition of ethanol–HCl–water mixture (130:0.24:0.5 ml) in thermostated bath at 0 °C, under continuous stirring. The final solution was kept at the same temperature for 30 min for complete hydrolysis, resulting in the TiO_2 sol. For the SnO_2 sol–gel preparation, tin tetrachloride pentahydrate (Acros) (12.37 g), was dissolved in isopropanol (Riedel-de Haën) (15 g) as the solvent. The hydrolysis step was carried out with the addition of distilled water (3.42 g) and isopropanol (10 g) under vigorous stirring. The resultant solution was allowed to aging overnight. Palladium addition to the TiO_2 and SnO_2 sols was performed by dissolving the corresponding amounts of palladium acetate (Aldrich) in the sol–gel mixtures to obtain 1% (w/w) PdO in TiO_2 and SnO_2 after calcination step.

The glass substrates were dip coated with sol–gel mixtures in five consecutive steps, each followed by drying at 120 °C for 20 min. Finally, the coated glass substrates were calcined in air at 650 °C for 10 min.

2.2. Characterization

The surface morphology of the coated substrates was investigated by scanning electron microscopy (SEM, Jeol JSM-6400). The absorption edge energies were measured by UV–vis spectrophotometer (Shimadsu, UV-1601) in the wavelength range of 290–550 nm. The XRD analyzes were performed with X-ray powder diffractometer (Philips, PW 1840) equipped with Cu target and Ni filter ($\lambda_{Cu\,K\alpha} = 1.5418$ nm).

The photochemical antibacterial activity of coated samples was measured against *E. coli*, *S. aereus*, *S. cerevisiae* cultures, and *A. niger spores*. Osram Ultra-Vitalux (Product Number: 003313) 300 W bulb with similar spectral distribution to solar spectrum between 280 and 780 nm was used as artificial irradiation source. The light intensity over the test bench was adjusted to achieve 10 mW/cm^2 within the visible range by adjusting the distance between the bench and light source.

E. coli (XL1-blue) and *S. aereus* were cultured aerobically in Luria–Bertani (LB) broth at 35 °C on a rotary shaker (170 rpm) overnight and were maintained on LB agar plates. The plates were incubated at 35 °C overnight and then stored at 4 °C until use. *S. cerevisiae* was cultured aerobically in YPD broth at 35 °C on a rotary shaker (170 rpm) for 24 h. *S. cerevisiae* was maintained on YPD agar plates. The plates were incubated at 35 °C for 24 h and then stored at 4 °C until use. *A. niger* was maintained on the potato-dextrose agar plates. The plates were incubated at 35 °C for 4 days until complete sporulation occurred. Spores were transferred and homogenized by vortexing in peptone water and directly used as the spore suspension for the inactivation tests. The microbial cell concentrations were determined before photocatalytic reactions by viable count procedure on agar plates after serial dilutions of the culture in 0.1% peptone water.

After cell counting, a solution of concentration of about 10^3 cells/ml was prepared by dilution in peptone water; 200 μl of the microbial suspension was pipetted onto the (19 cm^2) control surfaces and spread out to give a uniform and thin liquid film. Then, the samples were illuminated from above with artificial solar light and cell suspensions were removed from the surfaces at various time intervals. Removed suspensions were directly spread onto the agar plates and incubated at 35 °C for 16 and 24 h to determine the survivals of the bacteria and *S. cerevisiae*, respectively, by counting the colony-forming units (CFUs). *A. niger* spores were spread onto potato-dextrose agar (Merck) and incubated at 35 °C for 29 h to observe the growth of *A. niger*. Each evaluation was carried out at least in duplicate.

Controls: The effect of irradiation alone on the microorganisms and *A. niger* spores was determined on uncoated glasses. The effect of coating materials without photocatalysis on microbial growth was measured on coated samples in the dark. In addition, to determine the initial number of microbial cells that applied to surfaces, liquid cell suspension of 200 μl was spread onto agar plates and incubated at 35 °C. Empty agar plates were also incubated to test the sterilization conditions.

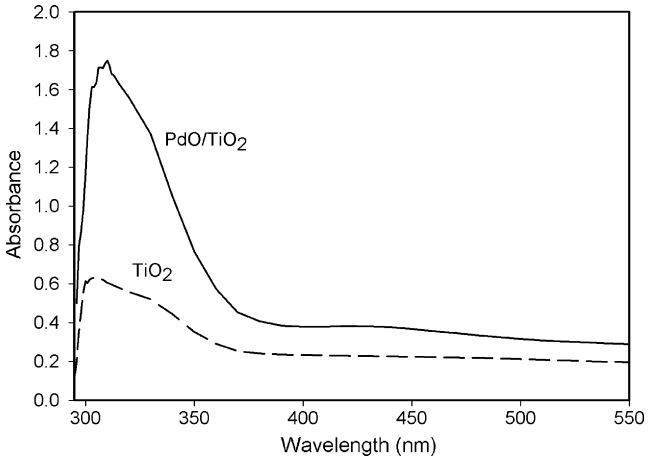

Fig. 1. UV–vis spectra of bare TiO_2 and PdO/TiO_2 samples.

3. Results and discussion

3.1. UV–vis analysis

UV–vis absorbance and reflectance spectroscopy of semiconductors contain valuable information in the sense of crystallite size, electronic properties of surface, oxidation states of species and metal support interactions. In Fig. 1, the UV–vis spectrum of both bare titanium dioxide (TiO_2) and 1% palladium over titanium dioxide (1% PdO/TiO_2) coated glass samples are given. During the analysis, bare glass slide was inserted in the reference channel of the spectrophotometer in order to cancel absorbance effects arising from the substrate. The absorption edge energy was determined by the linear regression and intersection of the lines fitted to the steep part of the UV–vis absorption and the baseline. As shown in Fig. 1, wide absorbance bands were obtained from both bare TiO_2 and 1% PdO/TiO_2 samples within the range of 295–370 nm. The intensity of absorbance for 1% PdO/TiO_2 is much higher than bare TiO_2 indicating the immense effect of metal addition even at 1% loading. The absorption edge energy of the bare TiO_2 was determined as 3.4 eV, which is attributed to the O^{2-}–Ti^{4+} [O (2p)–Ti (3d)] transition and this result shows that, there is 0.2 eV red shift compared with the literature value (3.2 eV) [57]. The 1% PdO/TiO_2 sample yielded 3.3 eV absorption edge energy which indicates that PdO addition enhances the conductance of sol–gel produced TiO_2 by 0.1 eV blue shift. The wide absorbance band with small intensity on 1% PdO/TiO_2 spectrum between 395 and 495 nm is assigned to Pd^{2+} d–d transitions or $Pd(O)n^{2+}$ clusters. The peak widening indicates that these clusters are very small and Pd^{2+} ions might be anchored to the surface oxygen of TiO_2 support. The Pd d–d transition occurs in two distinct band ranges as A (300 nm) and B (400 nm) [58,59]. The A (300 nm) band overlaps with the optical absorbance band of TiO_2 and is not resolved as a separate peak in the present case. However, the increase of absorbance on the 295–370 nm range can be associated with to d–d transition peak of Pd^{2+} ions.

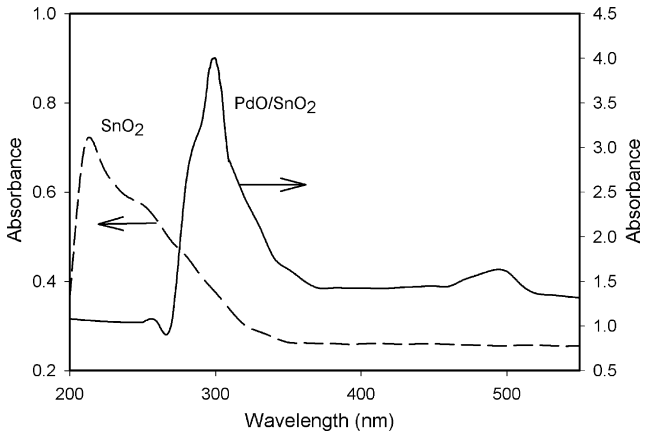

Fig. 2. UV–vis spectra of bare SnO_2 and PdO/SnO_2 samples.

Similarly, the optical absorbance of bare tin dioxide (SnO_2) and 1% palladium over tin dioxide (1% PdO/SnO_2) samples were analyzed. As observed from Fig. 2, a wide absorbance band between 200 and 360 nm was obtained for bare SnO_2 and between 270 and 360 nm for 1% PdO/SnO_2 samples. Similar to the TiO_2 based samples, 1% PdO doped sample yields much higher absorbance compared to the bare SnO_2 indicating the metal doping dominates the optical absorbance in the UV range. The most important point of this analysis is the wide blue shift of bare SnO_2 absorbance band to the higher energy, while the optical edge around 360 nm was observed for both SnO_2 and PdO/SnO_2 sample. The peak widening which extends asymmetrically to the blue (higher energy) indicates the inherent long-range disordered structure and the presence of smaller crystallites with more fragments and defects and; comparatively more amorphous structure exists over the bare surface of SnO_2 than the 1% PdO/SnO_2 surface. The absorption edge of bare SnO_2 was determined as 3.7 eV and this value represents +0.2 eV red shift with respect to the literature value (e.g. SnO_2 = 3.5 eV) [3]. The spectra of 1% PdO/SnO_2 represents that a completely different structure of PdO exists over the surface compared with the TiO_2 counterpart. The shoulder at 350 nm indicates the presence of dispersed Pd^{2+} ions and the sharp peak around 480 nm can be attributed to the isolated PdO crystallites over the SnO_2 surface which is typical for the PdO bulk phase. Similar results were also reported in literature [58,59]. These results reveal that PdO dispersion over the SnO_2 surface is not completely achieved and the surface contains both ionic Pd^{2+} species, which interacts with the O^{2-} ions of SnO_2 and larger isolated crystallites. The adsorption edge energy of 1% PdO/SnO_2 surface is determined as 3.6 eV, which indicates higher conductivity than the bare SnO_2 sample. The results of absorption edge energy analysis by UV–vis spectrophotometer indicated that both PdO promoted and bare samples of TiO_2 have superior conductivity than SnO_2 counterparts. The addition of 1% PdO to both TiO_2 and SnO_2 yields higher conductance, promotes the semiconductor properties and alters the optical absorbance character. Both SnO_2 and TiO_2 and their PdO doped counterparts are useful for photo-catalysis because of their validated semiconductor and optical properties.

3.2. Film morphology

The surface and particle morphology of the thin TiO_2 films which were produced by the five successive applications of sol–gel layers of TiO_2 over the glass substrate and heat treatment at 650 °C for 10 min were examined by SEM imaging. The samples were coated with gold, in order to achieve sufficient conductivity for analysis. The representative SEM images of TiO_2 films coated on glass substrates are given in Fig. 3(A and B). The formation of a continuous TiO_2 layer was observed over the samples that were examined and a smooth, glassy, defect free structure was the general appearance. At 20,000× magnification, where 50 nm resolution is achieved; neither particle structure, nor grains were observed over the surface. Fig. 4(A and B) represents the SEM micrographs of glass surfaces, coated with PdO/TiO_2 films, which were obtained after five-step coating of sol–gel solution and calcination at 650 °C for 10 min. The formation of smooth, homogeneous adhesion of the PdO/TiO_2 film was evidenced in these micrographs. It can be said that, the coating solution completely wetted the surface and well adhered to the glass surfaces and PdO doping had no adverse effect on the morphology of the TiO_2 thin films. Fig. 3(C and D) shows the surface SEM image of SnO_2 film, coated on the glass substrate. In overall, the SnO_2 film surface represents the grainy structure even at 2500× magnification. Although cracks as a result of shrinkage were observed from the figures, the coated underlayer can be seen from the grains over the surface. The overlap of five layers of coating may barely form a continuous SnO_2 matrix over the surface. This fact may lead to the loss of apparent electrical conductance over the surface (macro-range) as a result of 3–5 μm large gaps between the plate like structures, although the UV–vis analysis have proved the conductance of the samples in micro-range. Further analysis with higher magnifications (not shown) revealed that, SnO_2 films comprised of particles having 80–90 nm diameter [60], with a film thickness of 300–450 nm. It is believed that the shrinkages and cracks were due to the heat treatment step and large density difference between the sol–gel solution and SnO_2 solid film. Similar surface morphology was also observed for the PdO/SnO_2 samples (Fig. 4(C and D)). The crystal structure of SnO_2 and TiO_2 films were characterized by XRD technique with powder samples which are produced with the same procedure. The XRD analysis showed the anatase structure for TiO_2 and cassiterite (anatase) [60] structure of SnO_2 and their palladium doped counterparts.

3.3. Photocatalytic antimicrobial characteristics of the films

In order to characterize the antimicrobial efficiency of the films, microorganisms having different cell wall structures, namely *E. coli*, *S. aereus*, and *S. cerevisiae* besides *A. niger* spores, were selected. Control experiments, showing cell viabilities on uncoated glass surfaces with irradiation and on coated surfaces without irradiation have also been performed for all combinations of the microorganisms and coating types. Neither the coatings nor the illumination alone has any antimicrobial effect against the microorganisms.

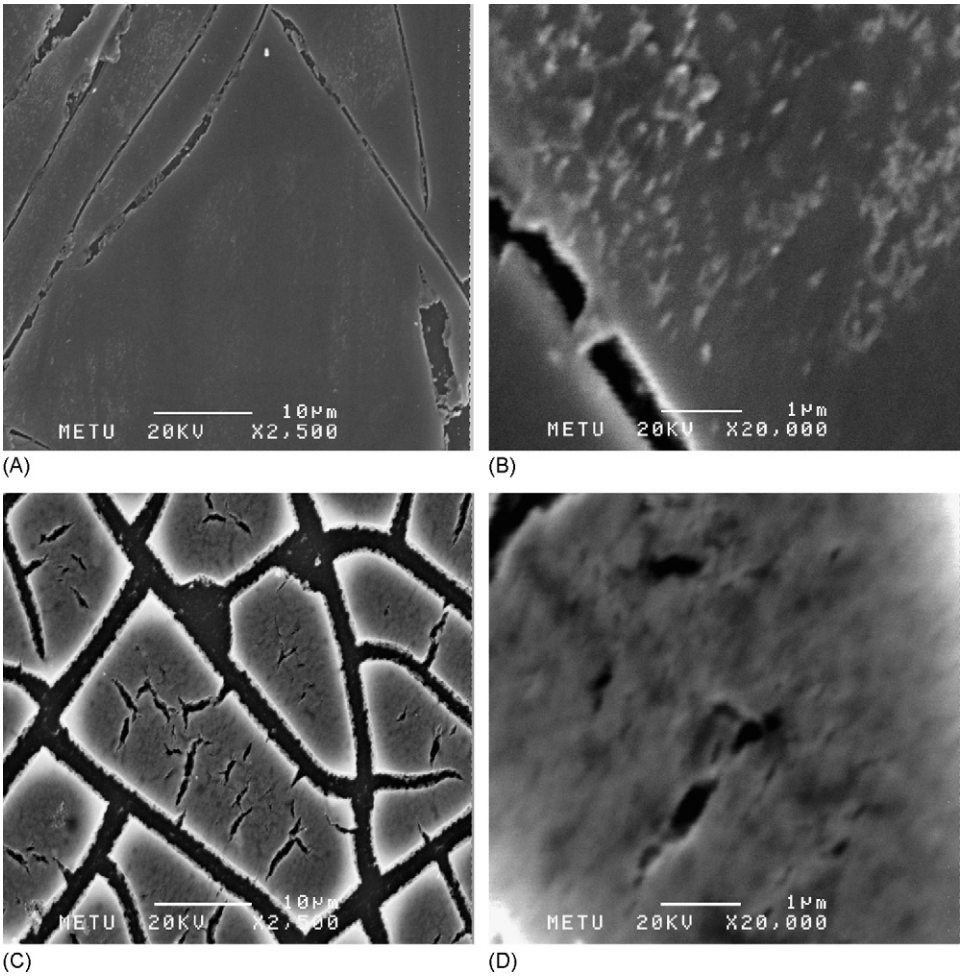

Fig. 3. SEM images of: (A), (B) TiO_2, (C), (D) SnO_2 films.

Fig. 5 shows the survival *E. coli* with respect to time under the 10 mW/cm^2 irradiation over bare, TiO_2, and PdO/TiO_2 coated glass surfaces. The number of *E. coli* cells over the TiO_2 coated glasses after 2 h of irradiation decreased by 85% as a result of photocatalytic inactivation. Higher inactivation rates, such as 99–100% within 1 h, for *E. coli* over TiO_2 have been reported [23,24]. However, inactivation rate is also dependent on light intensity and spectral distribution of irradiation source. In the present study, the inactivation tests were carried out with low light intensity at 10 mW/cm^2, in order to exclude the possible adverse effects of intense irradiation. The photocatalytic inactivation tests were also performed with PdO/TiO_2 films for *E. coli* under the same experimental conditions. In this case, 98% inactivation at the end of 2 h exposure was obtained indicating the enhanced photocatalytic inactivation as a result of PdO addition. The improved photocatalytic performance as a result of PdO addition might be attributed to the pronounced light absorption characteristics, and the presence of Pd^{2+} electron/hole pair traps [42,47,55,56].

The photocatalytic inactivation was modeled with first order kinetics under constant irradiation. The regression analysis yielded linear relation between the bacterial inactivation (ln (surviving fraction) versus time) with time. The first order rate constants of photocatalytic inactivation of *E. coli* cells were found as 0.017 and 0.023 min^{-1} for TiO_2 and PdO/TiO_2 coated glass samples, respectively.

The photocatalytic antibacterial properties of SnO_2 and PdO/SnO_2 coated glass samples were also tested to ensure the effect of palladium doping on semiconductor photocatalytic materials. Similar inactivation experiments were conducted with bare SnO_2 and PdO/SnO_2 coated glass samples against *E. coli*. As shown in Fig. 6, 56 and 68% inactivation of *E. coli* was observed on SnO_2 and PdO/SnO_2 films after 2 h irradiation, respectively. These inactivation results are lower than those of corresponding TiO_2 films, as expected due to the higher band gap energy and lower surface conductivity of SnO_2 than TiO_2. Similar to TiO_2, palladium doping on the SnO_2 semiconductor catalyst increased the photocatalytic activity. The first order kinetic analysis of the inactivation data against *E. coli* yield 0.007 and 0.008 min^{-1} for bare SnO_2 and palladium doped SnO_2 coated glass samples, respectively.

Different cell structures, particularly cell wall, are expected to play an important role in photocatalytic cell inactivation efficiency, since the cell envelope is the first barrier of the inactivation process [25]. Gr(+) bacteria are surrounded by a thick cell wall, typically 250 Å wide, composed of peptidogly-

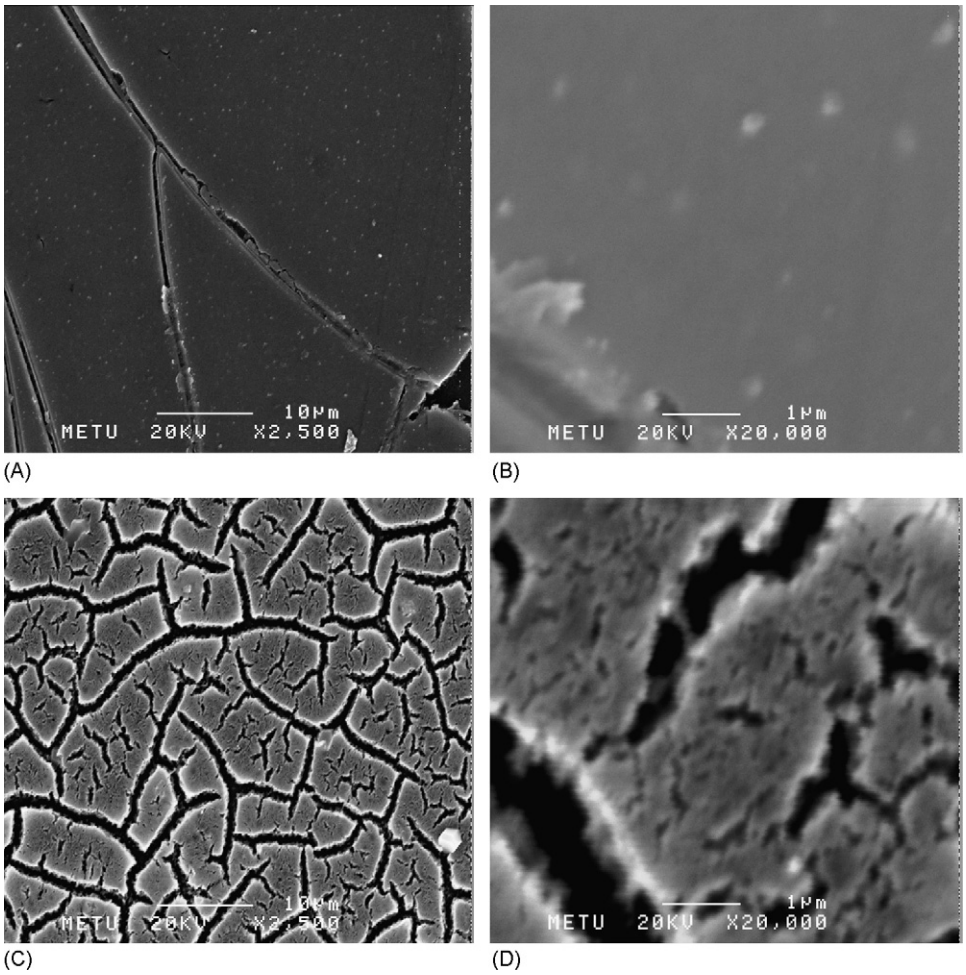

Fig. 4. SEM images of: (A), (B) PdO/TiO_2, (C), (D) Pd/SnO_2 films.

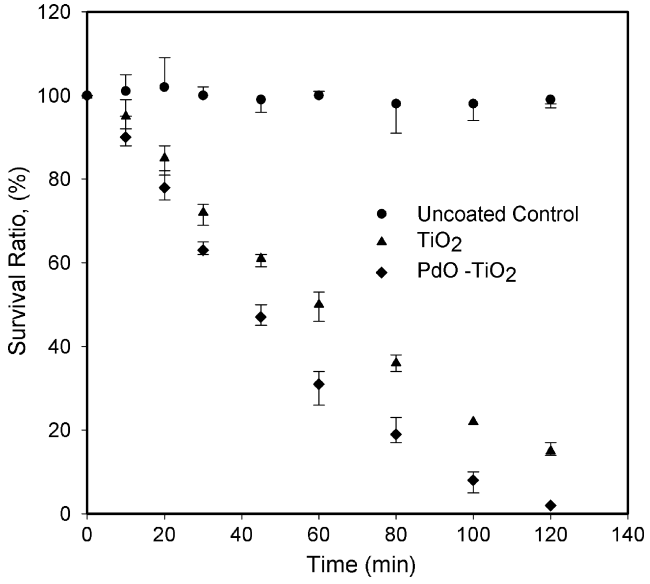

Fig. 5. Effect of irradiation time (10 mW/cm^2) on the survival ratio of *E. coli* over TiO_2 and PdO/TiO_2 films.

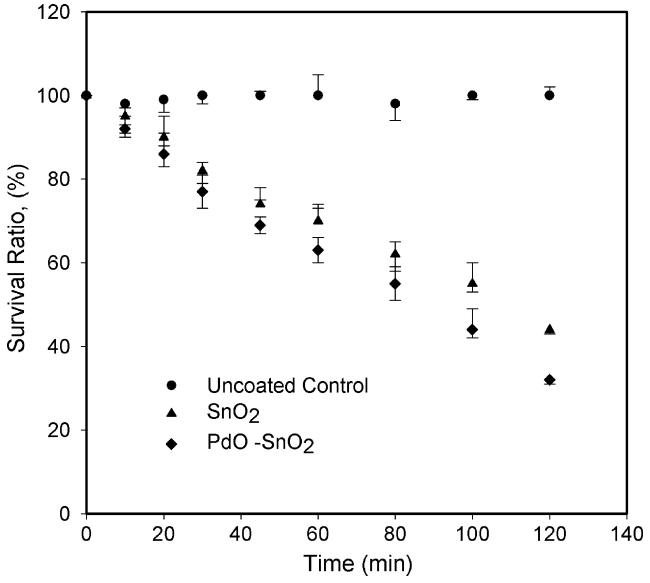

Fig. 6. Effect of irradiation time (10 mW/cm^2) on the survival ratio of *E. coli* over SnO_2 and PdO/SnO_2 films.

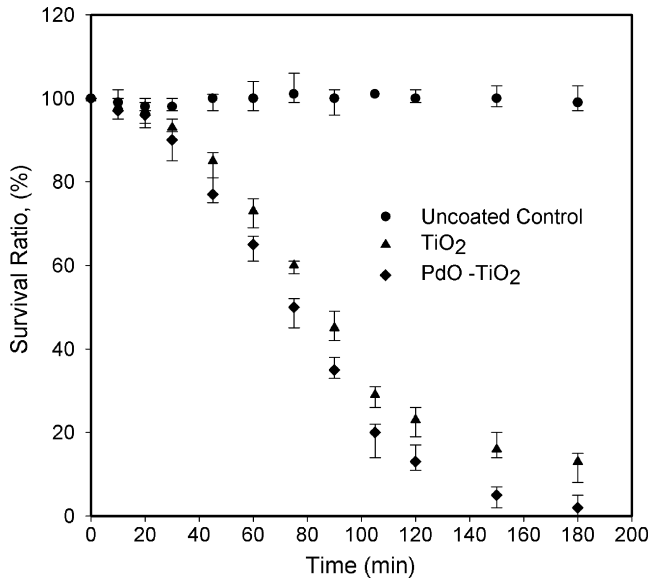

Fig. 7. Effect of irradiation time (10 mW/cm^2) on the survival ratio of *S. aureus* over TiO_2 and PdO/TiO_2 films.

can and teichoic acid whereas, Gr(−) bacteria are surrounded by a 30 Å-wide peptidoglycan wall, which in turn is covered by an 80 Å outer membrane that is a mosaic of protein, lipid and lipopolysaccharide [16]. Kiwi and Nadtochenko reported peptidoglycan layer as the most resistant cell wall/membrane component [12]. Therefore, photocatalytic inactivation experiments against *S. aureus*, which is a Gr(+) bacterium, were carried out for 3 h, considering its thicker and stronger cell wall structure. The inactivation test results against *S. aureus* over the TiO_2, SnO_2, and their palladium doped counterparts, were studied with uncoated glass control experiments and the results are given in Figs. 7 and 8. As observed from the figures, *S. aureus* inactivation is more elaborated with complex inactivation kinetics than *E. coli* where, three different regimes were observed. The inactivation of *S. aureus* exhibited a reverse S-shape trend with respect to time. The photocatalytic inactivation process starts with a slow initiation period, followed by a fast inactivation which eventually levels off. The complexity of inactivation kinetics might be attributed to the thicker and stronger cell envelope of Gr(+) bacterium than Gr(−). Like all Gr(−) bacteria, *E. coli* has an outer membrane and a thin cell wall, which could not protect the bacterium from photocatalytic oxidation thus, inactivation starts with irradiation immediately. Inactivation of the proteins and other molecules present in the outer membrane and periplasmic space of Gr(−) bacteria by photocatalytic oxidation may also be another reason of lower photocatalytic resistance of *E. coli*. After 3 h irradiation, 87 and 98% of *S. aereus* inactivation was achieved for TiO_2 and PdO/TiO_2, respectively. In the case of *E. coli*, the same degree of inactivation was observed after 2 h of irradiation. The kinetic analyses were also carried out for *S. aereus* for different regimes. The slow initiation period, which covers the first 30 min of irradiation, yields 0.004 and 0.007 min^{-1} for TiO_2 and PdO/TiO_2 coated glass samples, respectively. These rate constants are almost one-third of the rate constants that are evaluated for *E. coli*. However, the fast inactivation period between 30 and 100 min interval for *S. aereus* yields very similar rate constants to *E. coli* inactivation rates as 0.020 and 0.028 min^{-1} for TiO_2 and PdO–TiO_2 coated glass samples. Therefore, the first slow initiation period acts as a time lag for the inactivation process. With the use of SnO_2 and PdO/SnO_2 films, 79 and 90% inactivation of *S. aereus* were observed at the end of 3 h irradiation, respectively (Fig. 8). The kinetic analysis of inactivation of *S. aereus* over SnO_2 (0.004 min^{-1}) and PdO/SnO_2 (0.008 min^{-1}) yield very similar rate constants with TiO_2 counterparts for the slow initiation period which might suggest that, the inactivation kinetics is controlled by slow cell wall destruction step rather than the hydroxyl radical generation reactions. On the other hand, lower inactivation rate constants were observed for SnO_2 (0.012 min^{-1}) and PdO/SnO_2 (0.015 min^{-1}) coated glass samples than the TiO_2 coated ones within the 30 min–3 h region. Obviously, palladium addition contributes to higher antimicrobial activities for both SnO_2 and TiO_2. However, the antimicrobial efficiency of SnO_2 against *E. coli* is not higher than its efficiency against *S. aereus*, but similar inactivation degrees were achieved for both cases.

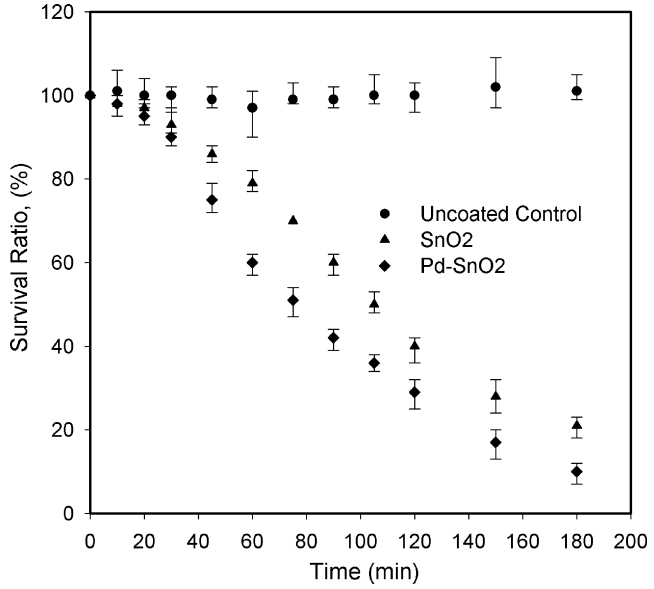

Fig. 8. Effect of irradiation time (10 mW/cm^2) on the survival ratio of *S. aureus* over SnO_2 and PdO/SnO_2 films.

Strength of the *S. cerevisiae* cell wall is high, which is mainly due to the inner layer of the wall that consists of β-D glucans and chitin. Together they represent 50–60% of the wall dry weight [17]. In addition, being an eukaryotic microorganism, its cell structure is more complex. So, in the microbial inactivation experiments against *S. cerevisiae*, the irradiation period was again increased to 3 h, as in the case of *S. aereus*. Microbial inactivation results against *S. cerevisiae* on TiO_2 and SnO_2 coated surfaces are given in Figs. 9 and 10, respectively. After 3 h illumination, 65 and 54% inactivation was observed against *S. cerevisiae* on the TiO_2 coated glasses with and without PdO, respectively (Fig. 9). The inactivation rate of *S. cerevisiae* was lower than the rates of both *E. coli* and *S. aereus* indicating the effect of the relatively complex morphology of an eukaryotic microorganism and strong cell wall. Additionally, the size of the

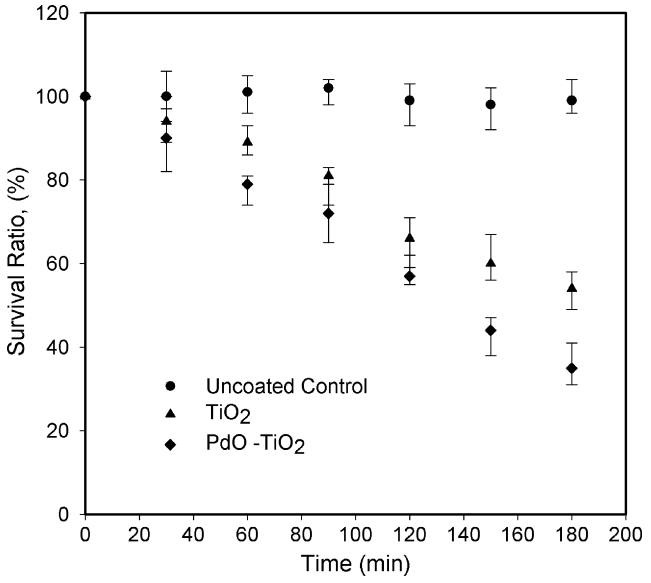

Fig. 9. Effect of irradiation time (10 mW/cm^2) on the survival ratio of *S. cerevisiae* over TiO_2 and PdO/TiO_2 films.

colonies following the irradiation treatment was much smaller than their initial size, suggesting the possibility of weakened survivors. Reduction of colony size was not observed either in the *E. coli* or *S. aereus* cases. Only 41 and 31% inactivation against *S. cerevisiae* was achieved with the photocatalytic effect of SnO_2 with and without PdO. These results are lower than those of TiO_2 surfaces as shown in Figs. 9 and 10. Again, very small sized colonies were observed over the SnO_2 coated samples. When the microbial cells, namely *E. coli*, *S. aereus* and *S. cerevisiae* were compared, the photocatalytic efficiency for the inactivation of *S. cerevisiae* was the lowest among all the samples. This result can also be deduced from the single regime inactivation kinetics having very low rate constants for *S. cerevisiae* which are evaluated as 0.004 (0.002) min^{-1} and 0.006 (0.003) min^{-1} for TiO_2 (SnO_2) and PdO/TiO_2 (SnO_2) samples. However, a fast inactivation regime following the slow step is not observed for *S. cerevisiae* like *S. aereus*, possibly showing not only the strong cell wall but also, complex eukaryotic cell structure are the rate limiting steps.

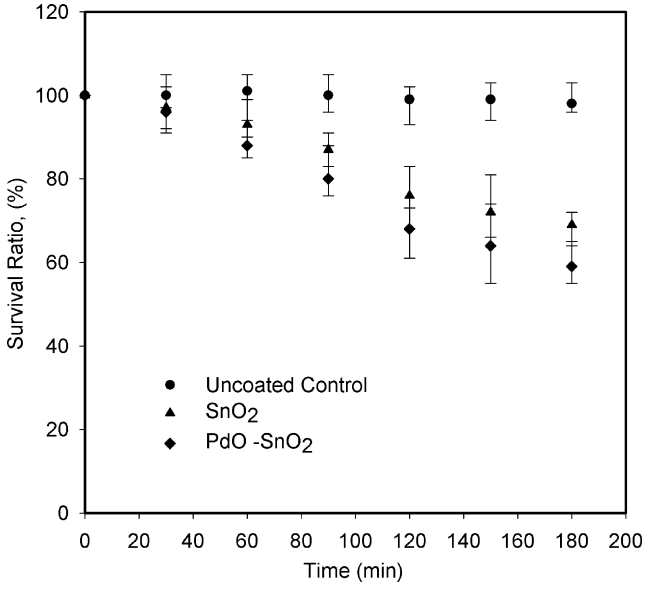

Fig. 10. Effect of irradiation time (10 mW/cm^2) on the survival ratio of *S. cerevisiae* over SnO_2 and PdO/SnO_2 films.

A. niger spore coats, similar to cell walls of the microorganism, contain chitin and glucan as the major polysaccharides [61,62]. These spores, having the capacity to survive drastic and stressful changes in their environment and to germinate after duration for long periods at difficult environments, are extremely resistant to adverse conditions [18]. Considering their high resistivity, the photocatalytic activities of all surfaces against *A. niger* spores were also investigated by prolonging the photocatalytic treatment up to 8 h. In these experiments, mycelium development on the agar plates was checked every hour during the incubation period, to observe any changes in the mycelium formation. Neither complete spore inactivation nor any major difference in mycelium development was observed over the course of photocatalytic inactivation treatment. This result is in agreement with the study by Wolfrum et al. [15] in which, 90% of *A. niger* spores was oxidized as a result of 72 h irradiation period [15].

4. Conclusions

The photocatalytic inactivation experiments with *E. coli*, *S. aereus*, and *S. cerevisiae* revealed that the addition of palladium oxide enhances the photocatalytic activity of both TiO_2 and SnO_2 thin films. The catalyst characterization studies with UV–vis spectroscopy showed an extension of absorption edge into visible region with the addition of 1 wt% PdO without altering the anatase structure of both SnO_2 and TiO_2. The positive effect of palladium addition was clearly observed and the best photocatalytic efficiency against all of the microorganisms, was achieved on 1 wt% PdO/TiO_2 coating. The antimicrobial properties of SnO_2 and PdO/SnO_2 coatings were less effective in photocatalytic microbial inactivation than TiO_2 and PdO/TiO_2 coatings, respectively. The antimicrobial efficiencies of the coatings against different microorganisms and fungal spores were found to decrease in the following order: *E. coli* > *S. aereus* > *S. cerevisiae* > *A. niger spores* for which, the complexity and strength of the cell walls increased in the same order. This order of precedence appears reasonable, if it is assumed that the primary step in photocatalytic decomposition consists of an attack to the cell wall. Existence of strong cell wall introduces high resistance to photocatalytic inactivation which manifests itself in terms of the slow initiation period hence, a time lag in the inactivation process. The highest antimicrobial efficiency was against *E. coli* presumably due to the simple and weaker cell structure.

References

[1] T. Matsunaga, R. Tomoda, T. Nakajima, H. Wake, FEMS Microbiol. Lett. 29 (1–2) (1985) 211–214.
[2] T. Saito, T. Iwase, J. Horis, T. Morioka, J. Photochem. Photobiol. B 14 (1992) 369–379.

[3] R. Benedix, F. Dehn, J. Quaas, M. Orgass, LACER 5 (2000) 157–167.
[4] J. Hong, M. Otaki, J. Biosci. Bioeng. 96 (3) (2003) 298–303.
[5] A. Fujishima, T.N. Rao, A.T. Donald, J. Photochem. Photobiol. C 1 (2000) 1–21.
[6] A.G. Rincon, C. Pulgarin, Catal. Today 101 (2005) 331–344.
[7] M. Cho, H. Chung, W. Choi, J. Yoon, Appl. Environ. Microbiol. 71 (2005) 270–275.
[8] A.G. Rincon, C. Pulgarin, Appl. Catal. B Environ. 44 (2003) 263–284.
[9] J.C. Sjorgen, R.A. Sierks, Appl. Environ. Microbiol. 60 (1994) 344–347.
[10] R.J. Watts, S. Kong, M.P. Orr, G.C. Miller, B.E. Henry, Water Res. 29 (1995) 95–100.
[11] P.C. Maness, S. Smolinski, D.M. Blake, Z. Huang, E.J. Wolfrum, W.A. Jacoby, Appl. Environ. Microbiol. 65 (1999) 4094–4098.
[12] J. Kiwi, V. Nadtochenko, Langmuir 21 (2005) 4631–4641.
[13] V.A. Nadtochenko, A.G. Rincon, S.E. Stanca, J. Kiwi, J. Photochem. Photobiol. A 169 (2005) 131–137.
[14] Z.X. Lu, L. Zhou, Z.L. Zhang, W.L. Shi, Z.X. Xie, H.Y. Xie, D.W. Pang, P. Shen, Langmuir 19 (2005) 8765–8768.
[15] E.J. Wolfrum, J. Huang, D.M. Blake, P.C. Maness, Z. Huang, J. Fiest, Environ. Sci. Technol. 36 (2002) 3412–3419.
[16] L. Stryer, Biohemistry, second ed., Freeman & Company, New York, 1981.
[17] A. Yiannikouris, J. François, L. Poughan, C.G. Dussap, G. Bertin, G. Jeminet, J.P. Joveny, J. Agric. Food Chem. 52 (2004) 3666–3673.
[18] R. Abrashev, P. Dolashka, R. Christova, L. Stenova, M. Angelova, J. Appl. Microbiol. 99 (2005) 902–909.
[19] O. Seven, B. Dindar, S. Aydemir, D. Metin, M.A. Ozinel, S. Icli, J. Photochem. Photobiol. A 165 (2004) 103–107.
[20] H.L. Liu, T.C.K. Yang, Process Biochem. 39 (4) (2003) 475–481.
[21] K. Sunada, T. Watanabe, K. Hashimoto, J. Photochem. Photobiol. A 156 (2003) 227–233.
[22] P. Amezaga-Madrid, G.V. Nevarez-Moorillon, E. Orrantia-Borunda, M. Miki-Yoshida, FEMS Microbiol. Lett. 211 (2002) 183–188.
[23] Z. Huang, P.C. Maness, D.M. Blake, E.J. Wolfrum, S.L. Smolinski, W.A. Jacoby, J. Photochem. Photobiol. A 130 (2000) 163–170.
[24] Y. Kikuchi, K. Sunada, T. Iyoda, K. Hashimoto, A. Fujishima, J. Photochem. Photobiol. A 106 (1997) 51–56.
[25] K.P. Kühn, I.F. Chaberny, K. Massholder, M. Stickler, V.W. Benz, H.G. Sonntag, L. Erdinger, Chemosphere 53 (2003) 71–77.
[26] T.A. McMurray, J.A. Byrne, P.S.M. Dunlop, J.G.M. Winkelman, B.R. Eggins, E.T. McAdams, Appl. Catal. A 262 (1) (2004) 105–110.
[27] J.R. Harbour, M.L. Hair, Adv. Colloid Interfaces 24 (1986) 103–141.
[28] J.C. Ireland, P. Klostermann, E.W. Rice, R.M. Clark, Appl. Environ. Microbiol. 59 (1993) 1668–1670.
[29] C. Ireland, J. Valinieks, Chemosphere 25 (3) (1992) 383–396.
[30] T.L. Xu, P.V. Kamat, K.E. O'Shea, J. Phys. Chem. A 109 (40) (2005) 9070–9075.
[31] I.A. Shkrob, M.C. Sauer Jr., J. Phys. Chem. B 108 (2004) 12497–12511.
[32] H.M. Coleman, M.I. Abdullah, B.R. Eggins, F.L. Palmer, Appl. Catal. B 55 (1) (2005) 23–30.
[33] T. Saito, T. Iwase, J. Horis, T. Morioka, J. Photochem. Photobiol. B 14 (1992) 369–379.
[34] P. Amezaga-Madrid, R. Silveyra-Morales, L. Cordoba-Fierro, G.V. Nevarez-Moorillon, M. Miki-Yoshida, E. Orrantia-Borunda, F.J. Solis, J. Photochem. Photobiol. B 70 (2003) 45–50.
[35] H. Sakai, E. Ito, R. Cai, T. Yoshioka, Y. Kubota, K. Hashimoto, A. Fujishima, Biochim. Biophys. Acta Gen. Subj. 1201 (1994) 259–265.
[36] Y. Koizumi, R. Yamada, M. Nishioka, Y. Matsumura, T. Tsuchido, M. Taya, J. Chem. Technol. Biotechnol. 77 (2002) 671–677.
[37] G. Dagan, M. Tomkiewicz, J. Phys. Chem. 97 (49) (1993) 12651–12655.
[38] P.V. Kamat, Pure Appl. Chem. 74 (9) (2002) 1693–1706.
[39] A.J. Bard, J. Photochem. 10 (1979) 59–75.
[40] P.V. Kamat, Chem. Rev. 93 (1993) 267–300.
[41] W.J. Albery, P.N. Bartlett, A. Hamnett, M.P. Dareedwards, J. Electrochem. Soc. 128 (7) (1981) 1492–1501.
[42] S.I. Shah, W. Li, C.P. Huang, O. Jung, C. Ni, PNAS 99 (2) (2002) 6482–6486.
[43] C.C. Trapalis, P. Keivanidis, G. Kordas, M. Zaharescu, M. Crisan, A. Szatvanyi, M. Gartner, Thin Solid Films 433 (1–2) (2003) 186–190.
[44] J.C.S. Wu, C.H. Chen, J. Photochem. Photobiol. A 163 (3) (2004) 509–515.
[45] C.G. Wu, C.C. Chao, F.T. Kuo, Cat. Today 97 (2004) 103–112.
[46] X. Wang, J.C. Yu, H.Y. Yip, L. Wu, P.K. Wong, S.Y. Lai, Chem. Eur. J. 11 (2005) 2997–3004.
[47] J. Arana, J.M.D. Rodriguez, J.A.H. Melian, E.T. Rendon, O.G. Diaz, J. Photochem. Photobiol. A 174 (2005) 7–14.
[48] M. Sheintuch, J. Schmidt, Y. Lecthman, G. Yahav, Appl. Catal. 49 (1) (1989) 55–65.
[49] M.M. Gadgil, R. Sasikala, S.K. Kulshreshtha, J. Mol. Catal. 87 (1994) 297–309.
[50] S.K. Kulshreshtha, R. Sasikala, Indian J. Chem. A 33 (2) (1994) 115–119.
[51] A. Boulahouache, G. Kons, H.G. Lintz, Appl. Catal. A 91 (2) (1992) 115–123.
[52] K. Grass, H.G. Lintz, J. Catal. 172 (2) (1997) 446–452.
[53] J.E. Drawdy, G.B. Hoflund, S.D. Gardner, E. Yngvadottir, D.R. Schryer, Surf. Interface Anal. 16 (1990) 369–374.
[54] D.R. Schryer, B.Y. Upchurch, B.D. Sidney, K.G. Brown, G.B. Hoflund, R.K. Herz, J. Catal. 130 (1) (1991) 314–317.
[55] B. Xie, Y. Xiong, R. Chen, J. Chen, P. Cai, Catal. Commun. 6 (2005) 699–704.
[56] S. Sakthivel, M.V., Shankar, M. Palanichamy, B. Arabindoo, D.W. Bahnemann, V. Murugesan, Water Res. 38 (004) 3001–3008.
[57] A.L. Linsebigler, G. Lu, J.T. Yates, Chem. Rev. 95 (1998) 735–758.
[58] D. Tessier, A. Rakai, B.F. Verduraz, J. Chem. Soc. Faraday Trans. 88 (1992) 741–749.
[59] A. Rakai, D. Tessier, B.F. Verduraz, New J. Chem. 16 (1992) 869–875.
[60] B. Mirkelamoglu, G. Karakas, Appl. Catal. A 281 (2005) 275–284.
[61] C.M. Stagg, M.S. Feather, Biochim. Biophys. Acta (BBA) Gen. Subject 320 (1973) 64–72.
[62] K. Horikoshi, S. Iida, Biochim. Biophys. Acta 83 (1964) 197–203.